Journal of Power Sources 511 (2021) 230395

Contents lists available at ScienceDirect

Journal of Power Sources

journal homepage: www.elsevier.com/locate/jpowsour

Structural and electrochemical trends in mixed manganese oxides $Na_x(M_{0.44}Mn_{0.56})O_2$ (M = Mn, Fe, Co, Ni) for sodium-ion battery cathode

Chol-Jun Yu [a,*], Yong-Chol Pak [a], Chung-Hyok Kim [a], Jin-Song Kim [a], Kum-Chol Ri [a], Kwang-Hyok Ri [a], Song-Hyok Choe [a], Stefaan Cottenier [b]

[a] Chair of Computational Materials Design (CMD), Faculty of Materials Science, Kim Il Sung University, Pyongyang, PO Box 76, Democratic People's Republic of Korea

[b] Department of Electromechanical, Systems and Metal Engineering & Center for Molecular Modeling (CMM), Ghent University, Technologiepark-Zwijnaarde 46, BE-9052 Gent, Belgium

GRAPHICAL ABSTRACT

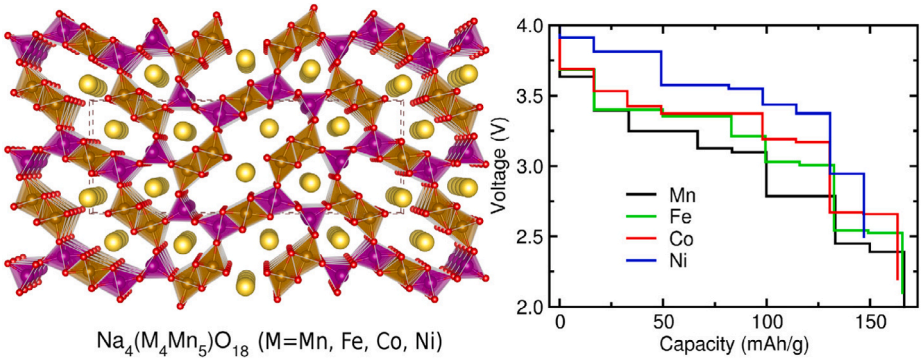

HIGHLIGHTS

- Sodium manganese oxides mixed with Fe, Co, Ni are suggested as improved cathodes.
- Compounds with certain formation energies have low volume expansion rates below 5%.
- Mixed compounds show increases of electrode voltage with high specific capacities.
- Compounds exhibit fast Na atom migrations along 1D pathways in S-shaped tunnel.
- Mixing enhances electron conductivity by improving the half-metallic behaviour.

ARTICLE INFO

Keywords:
Sodium-ion battery
Cathode
Sodium manganese oxide
Diffusion
First-principles

ABSTRACT

Developing cost-effective and high performance sodium-ion batteries (SIBs) relies mostly on advanced cathode materials with high electrode voltage, high capacity and fast sodium-ion diffusion. Here, we propose mixed sodium manganese oxides $Na_x(M_{0.44}Mn_{0.56})O_2$ (M = Mn, Fe, Co, Ni) as improved potential cathode materials for SIBs based on first-principles calculations. Our calculations reveal that these materials have relatively low volume expansion rates below 5%, and are thermodynamically stable. We find that the binding strength between the host and inserted Na atom gradually decreases as increasing the Na content x from 0.11 to 0.67 for each mixed compound, whereas it increases as going Mn→Fe→Co→Ni at each value of Na content. Identifying the intermediate phases during Na insertion/extraction, we find a slight increase of electrode

* Corresponding author.
E-mail address: cj.yu@ryongnamsan.edu.kp (C.-J. Yu).

https://doi.org/10.1016/j.jpowsour.2021.230395
Received 19 June 2021; Received in revised form 28 July 2021; Accepted 16 August 2021
Available online 3 September 2021

voltage with remarkably higher specific capacities by mixing due to extending the lower limit of Na content. We also investigate the sodium-ion diffusion by identifying plausible pathways and determining the activation barriers and diffusion coefficients, and find fast migration within the S-shaped tunnel and moderate one within the small-sized tunnel. Through analysis of density of states, we find that these compounds exhibit half-metallic behaviour, demonstrating an enhancement of metallicity by mixing with higher valent transition metal atoms. Our calculation results show that these mixed compounds can be advanced cathode materials for high performance SIBs.

1. Introduction

Gradually increasing demand for energy due to the ever-growing population has caused huge consumption of fossil fuels, leading to the growing concerns on serious global warming and climate change. Together with the related challenge of the gradual depletion of fossil fuel reserves, this is promoting concerted efforts to move toward renewable energy sources, such as solar and wind power. However, these natural energy sources often need robust, reliable and cost-effective energy storage devices such as lithium-ion and lithium sulphur batteries [1–4]. Sodium-ion batteries (SIBs) are triggering renewed interest as the most promising candidate for large-scale grid energy storage in light of the earth-abundance of Na resources, low cost of materials and high performance of batteries [5,6]. In advancing SIB technologies, the primary attention is being paid to developing and optimizing electrode materials that are capable of fast reversible Na ion insertion and extraction [7–9].

Sodium manganese oxides based on $Na_{0.44}MnO_2$ (NMO) are a highly promising cathode material for SIBs [10,11]. For its synthesis, various methods have been developed, including high temperature solid-state reaction [12–16], solution precursor method [17–20], spray pyrolysis [21], solution combustion synthesis [22,23], microemulsion method [24,25], and hydrothermal approach [26]. Regardless of what method is applied, NMO is usually obtained as nano-rods or nano-wires: long, one-dimensional (1D) crystallites. The relatively high electrochemical performance of this material is explained by it crystal structure, which shows large-sized and S-shaped tunnels, offering wide diffusion paths for a fast and reversible Na incorporation [16,27]. The sodium composition x in Na_xMnO_2 was found to be ranged from 0.22 to 0.66, giving the relatively high specific capacity of ~129 mAh g^{-1} with the Mn^{4+}/Mn^{3+} redox potential varying between 2.0 V and 4.0 V [11,19,28]. Moreover, the NMO structure is stable enough to be successfully applied with an aqueous electrolyte, indicating further cost reduction and safety improvement [27,29–31].

However, the rate performance and cycling stability are still insufficient at high rate, especially for the longer nano-rods or nano-fibres due to the poor Na diffusion behaviour. Shortening diffusion distance could be a way to address the problem, which can be achieved by optimizing the morphology, e.g., the shorter 1D nano-bars or 2D nano-plates [12]. On the other hand, Qiao et al. suggested that the Mn^{2+} formation on the NMO surface could be mainly associated with the capacity fading, and thus should be suppressed by controlling the electrode surface [22]. We face the questions; how high is activation barrier for Na diffusion and which pathway do Na ions follow in NMO? The questions can be solved by using first-principles method, as has been successfully applied to identifying the Na-intercalated phases in NMO [28].

For the transition metal oxides (TMOs) like NMO used for electrode materials for SIBs, intermixing was found to improve the structural stability and electrode performance. Intermixing of TMOs has been found mostly among Mn, Fe, Co and Ni oxides, such as binary [32–42], ternary [43–47], and quaternary [48,49] compounds. This is particularly appealing because Mn, Fe and Ni are abundant elements in the Earth's crust, they have a low cost and are environmentally friendly, while Mn-, Co-, and Ni-based electrodes exhibit high electrode potential with M^{3+}/M^{4+} redox couple. Such intermixing or ion replacing has also been proved to give enhanced electrode performance (capacity, voltage and stability) for polyanionic materials, including phosphates ($NaMPO_4$) or fluorophosphates ($NaMPO_4F$) [50–54], iron-based sulphates [55–58], and silicate cathodes [59]. Therefore, we are motivated to investigate the effect on the Na-ion diffusion and electrode performance of substituting a fraction of Mn in NMO with either Fe, Co or Ni.

In this work we will demonstrate that according to density functional theory (DFT) the NMO-based binary cathodes Na,x(M,0.44Mn, 0.56)O2 (M = Mn, Fe, Co and Ni) do indeed display a higher electrode voltage and a very fast ion diffusion, when compared to NMO itself. Here the Na content x is allowed to vary between 0.11 and 0.66, guaranteeing the high specific capacity and thus high energy density. We predict variation tendency of lattice constants and cell volume, formation enthalpy, and electrode potential by identifying the intermediate phases during Na insertion/extraction process in these compounds. Special attention is paid to uncovering the diffusion paths of Na-ion with calculation of the activation energies. To get an insight into electric current, the electronic density of states (DOS) are calculated.

2. Methods

2.1. Structural models

The crystal structure of $Na_{0.44}MnO_2$ is derived from $Na_4Mn_4Ti_5O_{18}$ which is in the orthorhombic system (space group $Pbam$) [60] with the lattice constants of a = 9.268 Å, b = 26.601 Å and c = 2.888 Å as first reported by Mumme [61]. When replacing Ti atoms fully by Mn atoms, the space group changes from $Pbam$ to $Pmc21$. In this structure, there are five different crystallographic sites for TM atoms, of which those on the M1 sites form the MO_5 square pyramids and those on the M2–M5 sites form the MO_6 octahedra, as shown in Fig. 1(a). These MO_x polyhedra are edge-shared along the crystallographic c-direction, forming the open tunnels with large-sized S-shape for Na diffusion on the Na1 and Na2 sites and small-sized pillar-shape for Na diffusion on the Na3 sites. We use the unit cell containing two formula units (62 atoms) for simulations of structural variation and voltage trends during Na insertion/extraction, and the supercell doubled in the c-direction for Na-ion diffusion. To make modelling of intermixing compounds, Mn^{3+} cations on the M1 and M4 sites of NMO are replaced by other TM atoms of Fe, Co and Ni, leading to the binary mixing compounds $Na_4(M_4Mn_5)O_{18}$ or $Na_{0.44}(M_{0.44}Mn_{0.56})O_2$ (NMMO), as shown in Fig. 1(b).

2.2. Computational details

DFT calculations were performed by using the pseudopotential plane-wave method as implemented in the Quantum ESPRESSO package (QE, version 6.2) [62]. The ultrasoft pseudopotentials were used to describe the ion–electron interaction.[1] The Perdew–Burke–Ernzerhof (PBE) [63] functional within the generalized gradient approximation (GGA) was used to take account of the exchange–correlation interaction between the valence electrons. To reasonably treat the localized 3d

[1] We use the ultrasoft pseudopotentials Na.pbe-sp-van_ak.UPF, Fe.pbe-sp-van_ak.UPF, Mn.pbe-sp-van.UPF, Co.pbe-nd-rrkjus.UPF, Ni.pbe-n-rrkjus_psl.0.1.UPF, and O.pbe-van_ak.UPF from http://www.quantum-espresso.org.

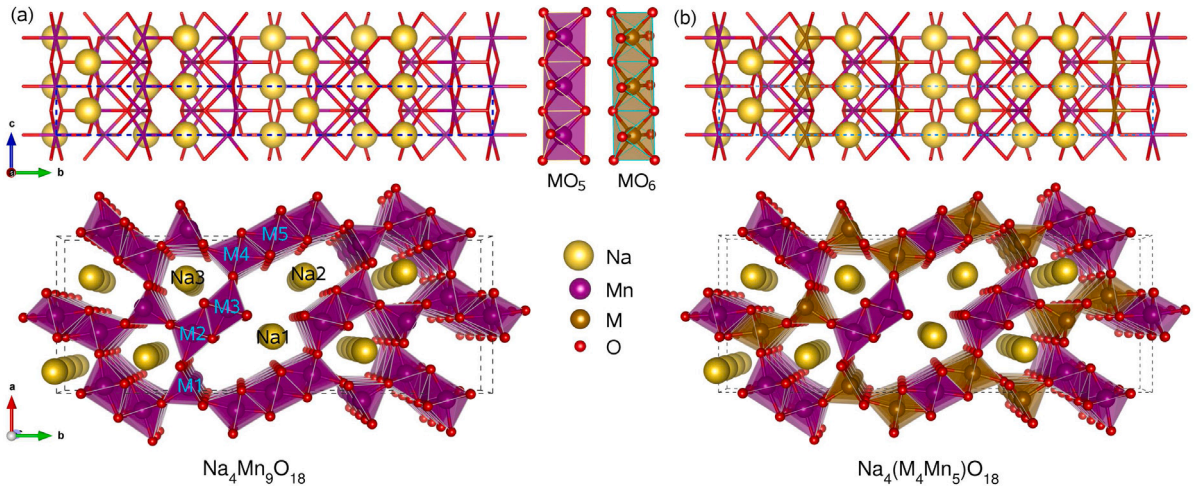

Fig. 1. Ball-stick (top panel) and ball-polyhedral (bottom panel) views for crystal structures of (a) sodium manganese oxide $Na_4Mn_9O_{18}$ and (b) intermixing binary oxides $Na_4(M_4Mn_5)O_{18}$ (M = Fe, Co, Ni). Transition metal (TM) atoms on M1 sites and M2–M5 sites build edge-sharing MO_5 square pyramids and MO_6 octahedra, forming the open tunnels with large-sized S-shape and small-sized pillar-shape for Na diffusion on the Na1 or Na2 and Na3 sites, respectively. Mn atoms on the M1 and M4 sites are replaced by other TM atoms of Fe, Co and Ni for making modelling of intermixing binary oxides. Dashed lines mark the unit cell.

electrons of TM atoms, DFT+U approach in the simplified version of Cococcioni and de Gironcoli [64] was applied with the on-site effective Hubbard U_{eff} (= $U - J$) parameters of 5.0, 4.5, 6.0 and 6.0 eV for Mn, Fe, Co and Ni, based on the Ceder et al.'s work [65]. Plane wave basis sets with kinetic energy cut-offs of 60 Ry and 600 Ry were used for expanding the wave functions and electron densities, respectively. To perform the Brillouin zone sampling for electron density calculation, special k-points with $(3 \times 2 \times 4)$ and $(6 \times 2 \times 8)$ meshes were used for structural optimization and DOS calculations, respectively. These computational parameters guarantee a total energy accuracy of 5 meV per formula unit. All atomic positions and lattice parameters were fully relaxed until the force on each atom and the pressure of crystalline lattice converged to 5×10^{-4} Ry Bohr^{-1} and 0.05 Kbar, respectively. Spin polarization was considered in the ferromagnetic (FM) configurations since these turned out to be lower in total energy than the antiferromagnetic configurations [28].

In the present form of NMO, the Mn cations are in +4 (on the M2, M3 and M5 sites) or +3 (on the M1 and M4 sites) oxidation states, and thus Na^+ ions can be inserted into or extracted from the host, allowing NMO to act as electrode active material with Mn^{4+}/Mn^{3+} redox couple. To roughly identify the positions of additional Na^+ ions and the paths for Na diffusion, we evaluated bond valence sum (BVS) for the Na–O bond using the formula, $B(\boldsymbol{r}) = \sum_i \exp[(1.803 - R_i(\boldsymbol{r}))/0.37]$ ($R_i(\boldsymbol{r}) = |\boldsymbol{r} - \boldsymbol{R}_i|$, $\boldsymbol{R}_i$ is the position vector of the ith atom) [66,67]. Then the exact diffusion paths, with the activation energies, were determined by applying the climbing image nudged elastic band (NEB) method [68] as implemented in the neb code of the QE package. While all the atoms were relaxed with fixing the supercell lattice parameters at the optimized values, NEB run with the seven image points was iterated until the force on the path converged to 0.05 eV Å^{-1}. Here DFT+U approach and spin polarizations were not considered, since their effects on the activation energy were negligible. Only Γ-point was used for saving computational time. Visualization of crystal structure and BVS isosurface plot was realized by using the VESTA code [69].

3. Results and discussion

3.1. Variation of lattice constants and volume

At the first onset, we optimized the unit cell of $Na_4Mn_9O_{18}$ or $Na_{0.44}MnO_2$, determining the lattice constants to be a = 9.060 Å, b = 26.208 Å and c = 2.793 Å in good agreement with the experimental values of a = 9.089 Å, b = 26.340 Å and c = 2.820 Å [12] within a relative error of 1%. This indicates that the computational settings in this work are reasonable, although our calculation with GGA+U gives slight underestimation in contrast to the general tendency of overestimation with the PBE functional within GGA.

Then, we determined the intermediate phases for further Na insertion into or extraction from NMO, corresponding to charge/discharge process in SIBs. For further Na insertion, two additional Na sites were identified in the S-shaped tunnel regions by plotting the difference of BVS (ΔBVS) which will be shown later (Fig. 4). Therefore, we could insert additional 4 Na atoms into the unit cell of $Na_4Mn_9O_{18}$ at the most, leading to the final compound of $Na_6Mn_9O_{18}$ (or $Na_{0.67}MnO_2$). This corresponds to the change of Mn charge state from $Mn_4{}^{3+}Mn_{5}{}^{4+}$ to $Mn_6{}^{3+}Mn_3{}^{4+}$. On the other hand, we considered that 6 Na atoms could be removed from the unit cell in this work, resulting in the compound of $NaMn_9O_{18}$ with the Mn charge state of $Mn^{3+}Mn_8{}^{4+}$, which was regarded as the initial compound for charge/discharge process. In this work, full removal of Mn was not allowed, because the resultant MnO_2 has completely different crystalline phase from NMO. After all, the Na content x in Na_xMnO_2 ranges from 0.11 to 0.67, and correspondingly the number of Na atoms n in $Na_nMn_9O_{18}$ varies between 1 and 6 with an interval of 0.5 in this study (see Figure S1 for crystal structure at each composition). In the previous work, the lower limit of x was set to be 0.19 [28], but we regarded that the possibility of realizing configuration with the least value of $x = 0.11$ should not be ruled out, provided that the phase is maintained during the Na extraction. The same composition range was also applied to the binary mixing oxides $Na_x(M_{0.44}Mn_{0.56})O_2$.

At each composition, we chose 10 configurations of Na ions with the lowest electrostatic energy by using the Ewald summation method and performed the structural optimizations to determine the lattice constants and the lowest formation enthalpy. The same Na ion configuration determined for NMO was used for the mixing oxides NMMO at each Na composition. Fig. 2 shows the determined lattice constants and cell volumes of $Na_x(M_{0.44}Mn_{0.56})O_2$ (M = Mn, Fe, Co and Ni) as varying the Na composition from 0.11 to 0.67 in comparison with the available experimental data for M = Mn case (see Table S1 for the values). The relative volume expansion rates $r_{\text{vol}} = (V_x - V_{1.0})/V_{1.0} \times 100\%$ were also estimated, since it can be an important factor for checking the cycling stability during the operation of SIBs.

We find that the variation trends are similar in overall appearance between them. For the whole range of Na composition x, the lattice constants a, b and cell volumes are shown to decrease as going Ni→Mn→Fe→Co. Similar tendency was observed in the polyanionic

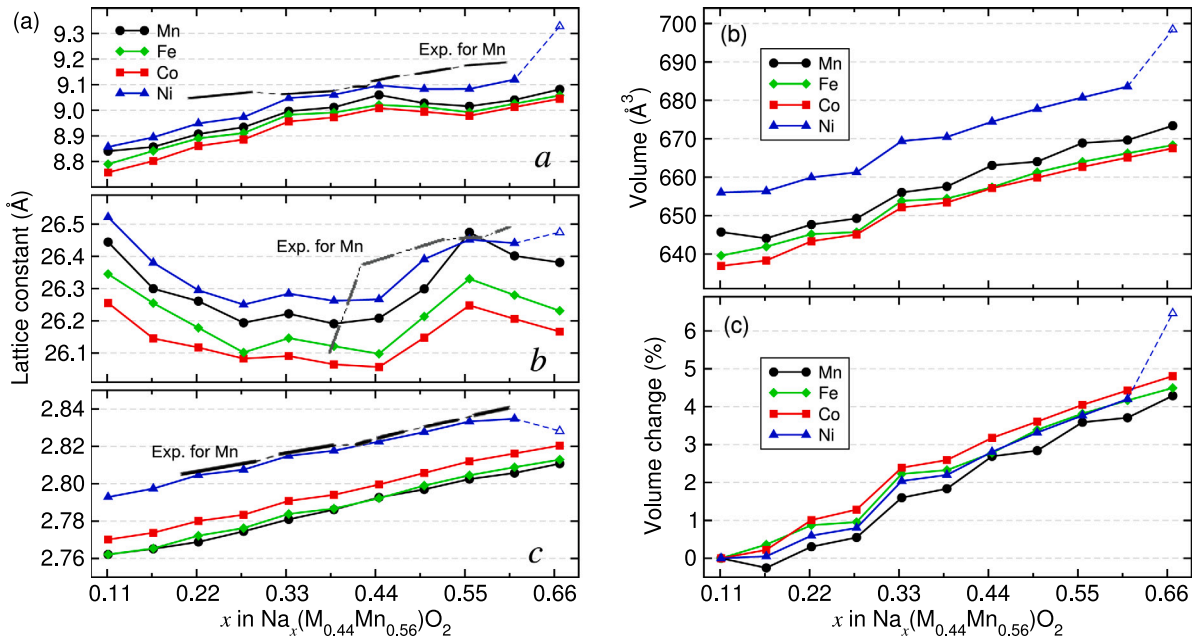

Fig. 2. Variation of (a) lattice constants (*a*, *b*, *c*), (b) unit cell volume, and (c) relative volume change rate $r_{vol} = (V - V_n)/V_n \times 100(\%)$ in $Na_x(M_{0.44}Mn_{0.56})O_2$ (M = Mn, Fe, Co, Ni) as increasing the Na content *x*. Experimental data for lattice constants of $Na_{0.44}MnO_2$ [28] are presented by solid-dashed lines.

compounds $Na_x(Fe_{0.5}M_{0.5})(SO4)_2$ (M = Mn, Co, Ni) [56] and Li_2MSiO_4 (M = Mn, Fe, Co, Ni) [59]. This is related with the average M–O bond lengths in MO_6 octahedra at M4 sites as 1.937, 1.891, 1.885 and 1.886 Å, and the average Mn–O bond lengths at M2, M3 and M5 sites as 1.896, 1.891, 1.891 and 1.890 Å for M = Ni, Mn, Fe and Co, of which ionic radii are 0.56, 0.58, 0.55 and 0.55 Å for M^{3+} in six-coordination [70]. On the other hand, the lattice constants *c* increase going Mn→Fe→Co→Ni, but the change extent is in the second decimal place, being much smaller than *a* and *c*. The relative volume expansion rates are in order of Mn→Ni→Fe→Co, but the differences between them are not so much.

The cell volumes for $Na_x(M_{0.44}Mn_{0.56})O_2$ were found to gradually increase as increasing the Na concentration *x* for all the four TM atoms. It is noteworthy that the maximal values of r_{vol} are below 5%, which is accepted as the threshold value for high cycle performance. The lattice constant *c* was also shown to monotonically increase as a function of Na content in accordance with the experimental data for NMO [28]. However, the lattice constants *a* and *b* exhibit the asymmetric change trends as the Na concentration increases, as have been reported by Sauvage et al. [16]. Interestingly, the change tendency of *a* is just contrary to that of *b*, such that from $x = 0.11$ to 0.44 *a* increases but *b* decreases, from 0.44 to 0.55 *a* decreases but *b* increases, and from 0.55 to 0.67 *a* increases but *b* decreases. These contrary change tendencies lead to the gradual increase of cell volumes due to the gradual increase of *c*. For the case of M = Ni, we find anomaly at $x = 0.67$, *i.e.* abnormal change of the lattice constants and cell volume. This is associated with the destruction of NiO_6 octahedra at M4 sites due to the significantly enlarged Ni–O bond length of 2.46 Å than the average M–O bond length of 1.94 Å (see Figure S2).

For extraction process from $x = 0.44$ configuration, the Na atoms at the Na3 sites (small-sized pillar-type tunnel) began to extract and arrived at the complete extraction at $x = 0.22$ composition. Subsequently, the Na2 site atoms (large-sized S-type tunnel) were removed from the lattice. Finally, only the Na1 site atoms remained at $x = 0.11$. Meanwhile, the insertion into $x = 0.44$ configuration began to fill the vacant Na2 sites as going from $x = 0.44$ to $x = 0.55$. Finally, the vacant Na1 sites were filled at $x = 0.67$ (see Figure S1 for the intermediate structures). From such Na extraction/insertion process, the Na–O binding can be said to get stronger as going Na3→Na2→Na1 sites.

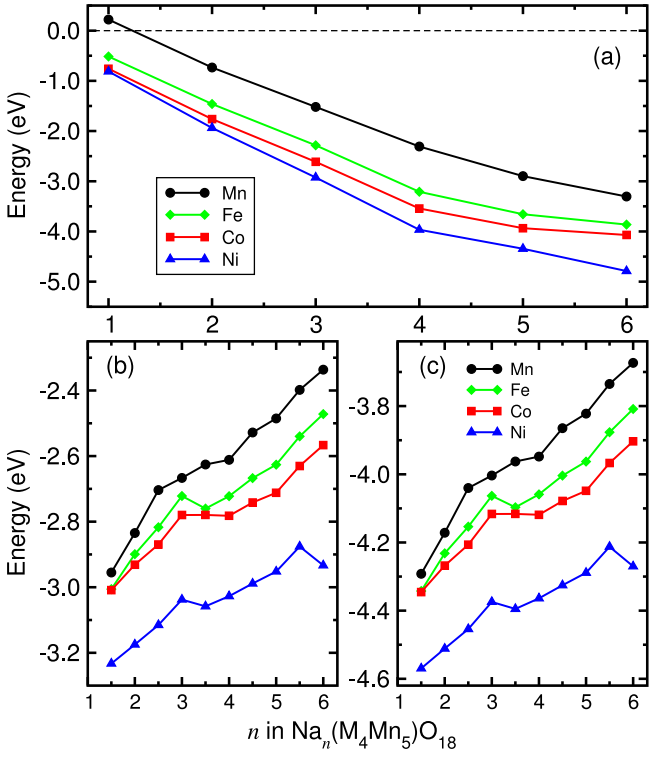

Fig. 3. (a) Formation energy per formula unit of $Na_n(M_4Mn_5)O_2$ (M = Mn, Fe, Co, Ni) from constituent metal oxides, (b) formation energy per Na atom from the host ($n = 1$ compound) and Na metal in *bcc* phase, and (c) binding energy per Na atom between the host and inserted Na atoms, as increasing the number of Na atoms.

To get more insight into structural stability, we calculated the Jahn–Teller distortion parameters of MO_6 octahedra, such as mean quadratic elongation $\lambda_{oct} = \frac{1}{6}\sum_{i=1}^{6}(l_i/l_0)^2$, bond angle variance $\theta^2_{oct} = \frac{1}{12}\sum_{i=1}^{12}(\theta_i - 90)^2$, and bond length distortion index $DI = \frac{1}{6}\sum_{i=1}^{6}|l_i/l_0 - 1|$ [71]. Here, l_i is the M–O bond length in the distorted octahedral MO_6, l_0

is the M–O bond length in MO_6 octahedra with O_h symmetry and volume equal to that of the distorted octahedra, and θ_i is the O–M–O bond angle, respectively. In an ideal undistorted octahedral MO_6, the distortion parameters are $\lambda_{oct} = 1$, $\theta^2_{oct} = 0$, and $DI = 0$. For M2–M5 sites, we calculated the distortion parameters (see Table S4). It was known that partial divalent Ni doping into P2-Na_xMnO_2 can effectively eliminate Mn^{3+} and alleviate the Jahn–Teller effect, which can degrade the structure stability [72]. Likewise, it was found in this work that replacing Mn^{3+} on M4 sites with Fe, Co and Ni reduced the λ_{oct} values for M2, M3 and M5 sites, θ^2_{oct} value for M2 and M3 sites, and DI values for M3 and M5 sites. These resulted in reduction of Jahn–Teller distortion, leading to an enhancement of structural stability on cycling.

3.2. Energetics and electrode voltage

We checked formability of $Na_n(M_4Mn_5)O_{18}$ compounds by calculating the formation energy from the constituent binary metal oxides including Na_2O, M_2O_3 and MO_2 (see Table S2 and S3 for the corresponding chemical reactions and crystalline information of metal oxides). As shown in Fig. 3(a), the formation energies were calculated to be negative for all the compounds in the whole range of Na number from $n = 1$ to $n = 6$, indicating certain possibility of their formation. Only an exception of positive value 0.22 eV per formula unit was observed for $NaMn_9O_{18}$, which is therefore considered to be unstable. It was found that the formation energy increases in magnitude, both upon increasing the number of inserted Na atoms (irrespective of the mixed transition metal), as well as upon increasing the atomic number of the transition metal atom at each value of Na composition, thereby indicating the enhancing structural stability.

The binding strength between the inserted Na atoms and the host compound, which is the starting compound with $n = 1$ in this work, can be assessed by the formation energy per Na atom from the host and Na metal in body-centred cubic (bcc) phase as $E_f = \frac{1}{n}[E_{Na_{1+n}MMO} - (E_{NaMMO} + nE_{Na_{bcc}})]$ or the binding energy per Na atom as $E_b = \frac{1}{n}[E_{Na_{1+n}MMO} - (E_{NaMMO} + nE_{Na_{atm}})]$, where E_{Na_nMMO}, $E_{Na_{bcc}}$ and $E_{Na_{atm}}$ are the total energies of $Na_n(M_4Mn_5)O_{18}$, bcc-Na metal and isolated Na atom, respectively. As shown in Fig. 3(b) and (c), both the formation and binding energies, being negative for the whole range of Na content, generally decrease in magnitude as increasing the number of inserting Na atoms into the host. Moreover, the binding strength was shown to be gradually enhanced as going Mn→Fe→Co→Ni in accordance with the change tendency of lattice constant c. For M = Ni, the formation and binding energies were shown to be abnormally reduced when $n = 6$, being related with the abnormal change of cell structure. These indicate that replacing some Mn atoms in NMO with other TM atoms of Fe, Co and Ni clearly enhances the structural stability and binding strength. This is quite beneficial to the SIB operation.

The relative stability of intermediate phase upon insertion or extraction of Na atoms into the starting host $Na(M_4Mn_5)O_{18}$ or from the ending compound $Na_6(M_4Mn_5)O_{18}$ was estimated by evaluating its formation energy with respect to the two end compounds as follows,

$$\Delta H_f = E_{Na_{1+n}MMO} - [(1-x)E_{NaMMO} + xE_{Na_6MMO}] \quad (1)$$

where $x = n/5$ and n varies between 0 and 5. Fig. 4(a) shows the convex hull plot for formation enthalpies calculated from the numerous different Na configurations. For the case of M = Ni, we also drew the convex hull plot obtained by using the $n = 5.5$ compound as the end one, since the $n = 6$ compound exhibits the disrupted MO_6 octahedra. The numbers of stable intermediate phases, *i.e.*, those lying on the convex hull, were identified to be 7, 7, 7, and 6 for M = Mn, Fe, Co, and Ni, respectively.

Using these intermediate phase, we estimated the step discharge voltage between the adjacent Na contents with respect to Na/Na^+ counter electrode as follows,

$$V = -\frac{E_{x_j} - E_{x_i} - (x_j - x_i)E_{Na_{bcc}}}{e(x_j - x_i)} \quad (2)$$

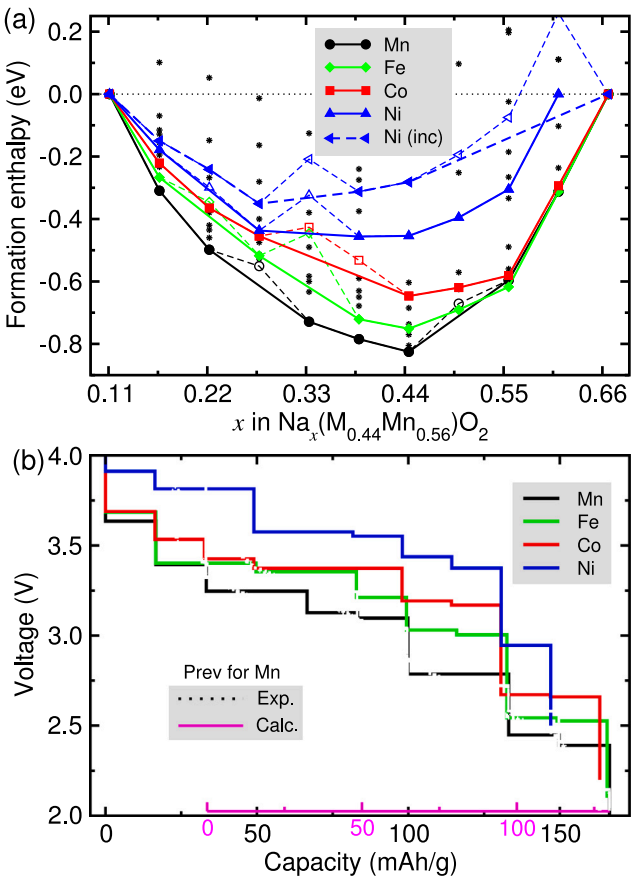

Fig. 4. (a) Convex hull plot for formation enthalpies of as a function of Na content x (= 0.11–0.67) and (b) electrode voltage calculated using the intermediate phases identified by the convex hull as a function of specific capacity in $Na_x(M_{0.44}Mn_{0.56})O_2$ (M = Mn, Fe, Co, Ni). Experimental and calculation data for M = Mn with the x = 0.22–0.67, which gives the specific capacity of 129.4 mAh g^{-1}, are also provided from Ref. [28].

where E_{x_j} and E_{x_i} are the total energies of $Na_x(M_{0.44}Mn_{0.56})O_2$ compounds with $x = x_j$ and $x = x_i$, and e is the elementary charge. Fig. 4(b) shows the electrode voltage steps for the four kinds of mixing compounds as functions of capacity. We found a systematic increase of electrode voltage as increasing the atomic number of TM atoms (see Table 1). The specific capacity is an important factor determining the energy density of batteries. Experimentally, the Na content x was found to range from 0.22 to 0.67 for NMO, giving the theoretical capacity of 129.4 mAh g^{-1}. Our calculation was confirmed to agree with the previous experimental and computational data for NMO [28]. As discussed above, the range of x is extended as from 0.11 to 0.67 or 0.61 for binary mixing compounds due to their negative formation energies from the metal oxides, thereby increasing the specific capacity to 165.6, 163.2 and 147.0 mAh g^{-1} for M = Fe, Co and Ni, respectively. Considering that the energy density is also affected by the electrode voltage, intermixing of Mn in NMO with Fe, Co and Ni was found to be able to provide higher energy density due to higher electrode voltage and higher capacity.

3.3. Sodium-ion diffusion

Next, we investigated the diffusion properties of Na^+ ion, which determine one of the key factors for assessing suitability of electrode material, the rate capability of SIBs. The diffusion properties include the way of Na diffusion, diffusion length, activation energy and diffusion coefficients. In order to start doing this work, we first identified the

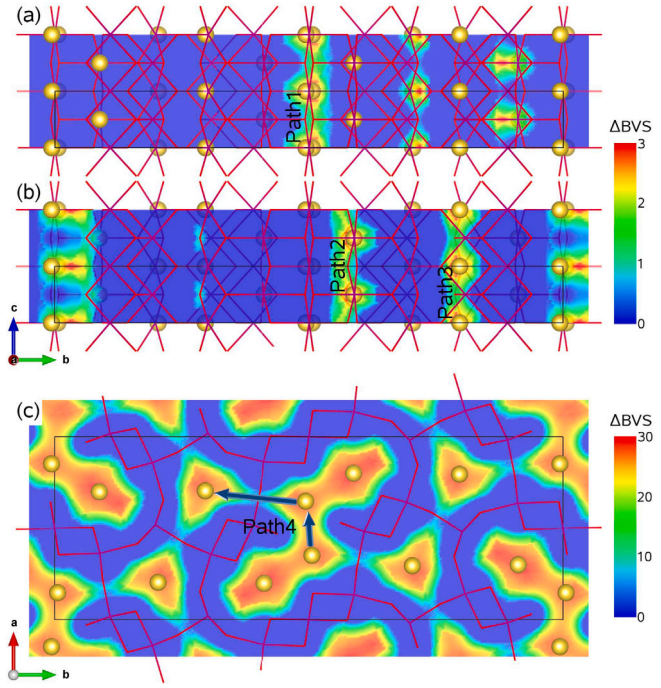

Fig. 5. Contour plot of ΔBVS on (a) middle (100) plane, (b) top (100) plane, and (c) (001) plane for identifying plausible four pathways of Na-ion migration, marked as Path1, Path2 and Path3 within S- and pillar-shaped tunnels, being parallel to the c direction, and three-dimensional Path4 across the tunnels.

plausible pathways for Na ion migration by estimating ΔBVS for Na atoms and plotting its contour map, as shown in Fig. 5 for $Na_{0.44}MnO_2$. Through the analysis of ΔBVS plot, four different pathways were identified to be possible; Path1 and Path2 for Na1 and Na2 sites within the S-shaped large tunnel, Path3 for Na3 site within the small-sized tunnel, and Path4 for migration from Na1 to Na3 sites across the tunnels. The Path1, 2 and 3 are characterized by 1D channel within the tunnels, being parallel to the c direction, whereas the Path4 is 3D pathway. Moreover, the 1D-type paths could be identified with low ΔBVS value of 3 while the Path4 by higher value of 30, indicating that the Path4 may be difficult to actually occur.

Then, we determined the actual diffusion lengths and activation barriers for Na-ion migration along these pathways by applying the NEB method to the $Na_{0.44}$MMO intermixing compounds. Here, the Na-ion migrations were suggested to follow the vacancy-mediated mechanism. Fig. 6 shows the determined configurations during the Na migrations along the pathways together with the corresponding activation energies. For the case of $Na_{0.44}MnO_2$, we tested all the four different pathways and presented the migration paths with the activation energies in Fig. 6(a) and (b). As was expected, the Na-ion diffusion within the large S-shaped tunnel along the Path1 and Path2 was easier to occur with lower activation barriers (0.37 and 0.07 eV) than that within the small-sized tunnel along the Path3 (0.44 eV). In particular, the activation barrier for the Path2 migration on the Na2 site was found to be remarkably low as 0.07 eV, indicating very fast Na^+ ion migration along this channel. The diffusion lengths were found to be somewhat similar as about 3.0 Å. The Na ion diffusion across the tunnel along the Path4 is not likely to occur due to its relatively higher activation energy of 0.68 eV. Therefore, it can be said that the Na ion insertion/extraction in NMO occurs on the Na1, Na2 and Na3 sites separately along the 1D pathways within the tunnels without happening of interchange between the different Na sites.

For the intermixing NMMO compounds, we tested the low activation barrier pathways of Path1, Path2 and Path3. Fig. 6(c) shows the energy profiles along the pathway of Path1 calculated by using the

Table 1
Electrochemical properties of intermixing compounds $Na_x(M_{0.44}Mn_{0.56})O_2$ (M = Mn, Fe, Co, Ni), including relative volume change rate r_{vol}, specific capacity C, electrode voltage U, activation barrier E_a along the Path1 and Path2, and Na ion diffusion coefficient D. Values in parenthesis are obtained with $x = 0.11 - 0.66$.

M	r_{vol} (%)	C (mAh g^{-1})	U (V)	E_a (eV)	D (cm^2 s^{-1})
Mn	4.29	129.4	3.64–2.39	0.367	3.36×10^{-12}
		(166.4)		0.069	3.76×10^{-7}
Fe	4.49	165.6	3.68–2.53	0.371	2.87×10^{-12}
				0.076	2.85×10^{-7}
Co	4.81	163.2	3.69–2.66	0.412	6.04×10^{-13}
				0.083	2.27×10^{-7}
Ni	4.20	147.0	3.91–2.95	0.431	3.22×10^{-13}
	(6.46)	(163.4)		0.109	1.04×10^{-7}

NEB approach. The activation barriers were determined to gradually increase from 0.367 to 0.431 eV with increasing the number of TM atoms, while the diffusion lengths were found to be similar as about 2.88 Å for Mn, Fe and Co but the longer value of 3.06 Å was observed for Ni. Also, systematic tendencies were observed for activation barriers along the pathways of Path2 as it gradually increases as 0.069, 0.076, 0.083 and 0.109 eV for Mn, Fe, Co and Ni with increasing diffusion lengths of 3.01, 3.02, 3.05 and 3.41 Å as shown in Fig. 6(d) (see Figure S3 along the Path3). The Na-ion diffusion coefficients were obtained by $D = a^2 \nu \exp(-E_a/k_B T)$ with diffusion length for a, $\nu = 6\times10^9$ Hz, and the calculated activation energy E_a at room temperature ($k_B T = 0.026$ eV) (see Table 1). These indicate that the electrostatic repulsion between TM and Na cations is clearly pronounced for Na diffusion along the tunnel pathways. We summarize the structural and electrochemical properties of the mixing compounds in Table 1.

3.4. Electron conductivity

Finally, we calculated the electronic density of states (DOS) to get an insight into the electron conductivity of the electrode. During charge/discharge process, electrons travel through the external circuit and merge with the Na^+ ions in the electrode. Therefore, electrode materials of alkali ion batteries should possess good electron conductivity, otherwise conductive agent such as carbon black should be included in making electrode. Fig. 7 shows the atom-resolved DOS for $Na_{0.44}$MMO calculated by using GGA+U method with FM spin configuration. For $Na_{0.44}MnO_2$, a very narrow band gap of 0.25 eV was found for spin-up states contributed by hybridization of Mn 3d and O 2p states, but a wide band gap of 3.78 eV was obtained for spin-down states, where the valence band (VB) states are originated dominantly from O 2p states and the conduction band (CB) states are from Mn 3d and a small amount of O 2p states (see Figure S4 for t_{2g} and e_g orbital-projected partial DOS from Mn 3d states). This agrees with the previous calculation [28], and indicates that NMO belongs to half-metallic oxides [73]. Such half-metallic behaviour remains almost unchanged for Na_xMnO_2 with increasing ($0.44<x\leq0.67$) or decreasing ($0.11\leq x<0.44$) Na concentration (see Figure S8). Therefore, it should be noted that electric current in NMO is fully spin polarized and the applied magnetic as well as electric field may affect the electron transfer.

When mixing NMO with other TM atoms, no band gaps were observed for spin up channel, and moreover, the band gap for spin down channel was found to decrease such as 2.59, 1.62 and 1.95 eV for Fe, Co and Ni, respectively. In these mixing $Na_{0.44}$MMO compounds, the spin up states around the Fermi level comprise the hybridization of O 2p with Mn and other TM 3d states, whereas the spin down states are contributed mainly by TM 3d states with a certain amount of O 2p states (see Figures S5–S7 for t_{2g} and e_g orbital-projected partial DOS from TM 3d states). These indicate that replacing some Mn atoms by Fe, Co and Ni enhances metallicity of half-metallic NMO, possibly due to increasing number of 3d electrons of TM elements. This can improve the electron transferability and so electrode performance of SIBs.

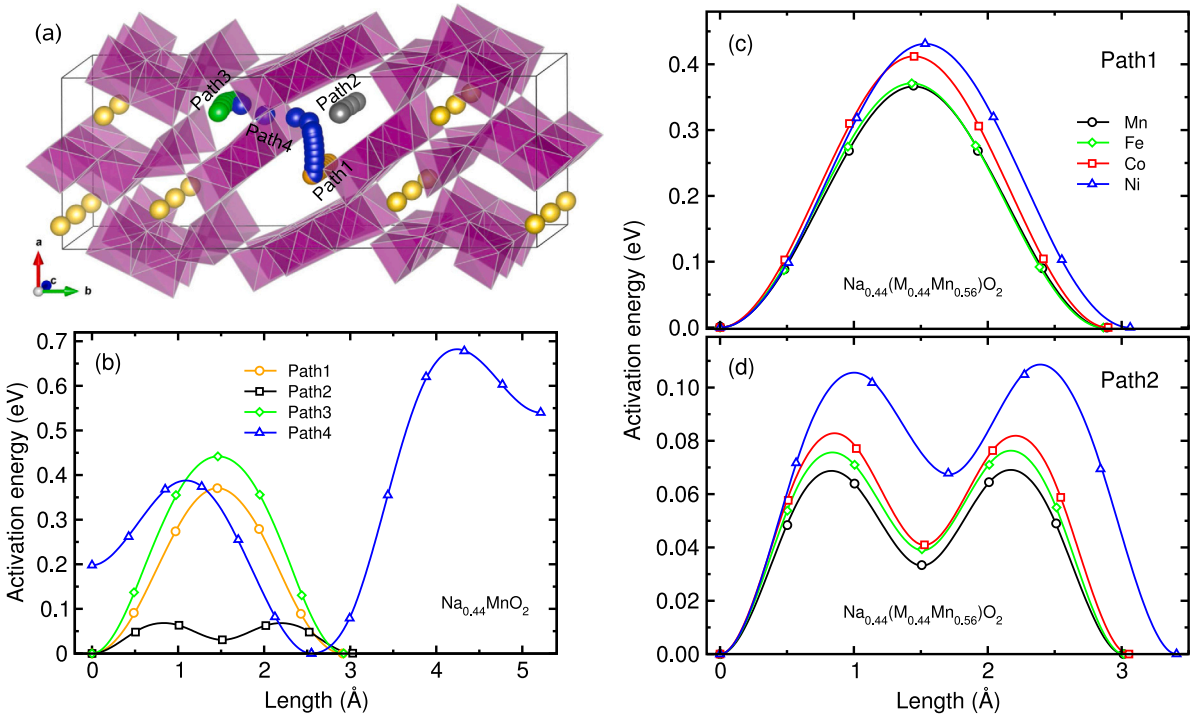

Fig. 6. (a) Ball and polyhedral view of Na-ion migration along the different pathways of Path 1–4, and (b) corresponding activation energy in $Na_{0.44}MnO_2$. Activation energies along (c) Path1 and (d) Path2 in $Na_{0.44}(M_{0.44}Mn_{0.56})O_2$ (M = Mn, Fe, Co, Ni).

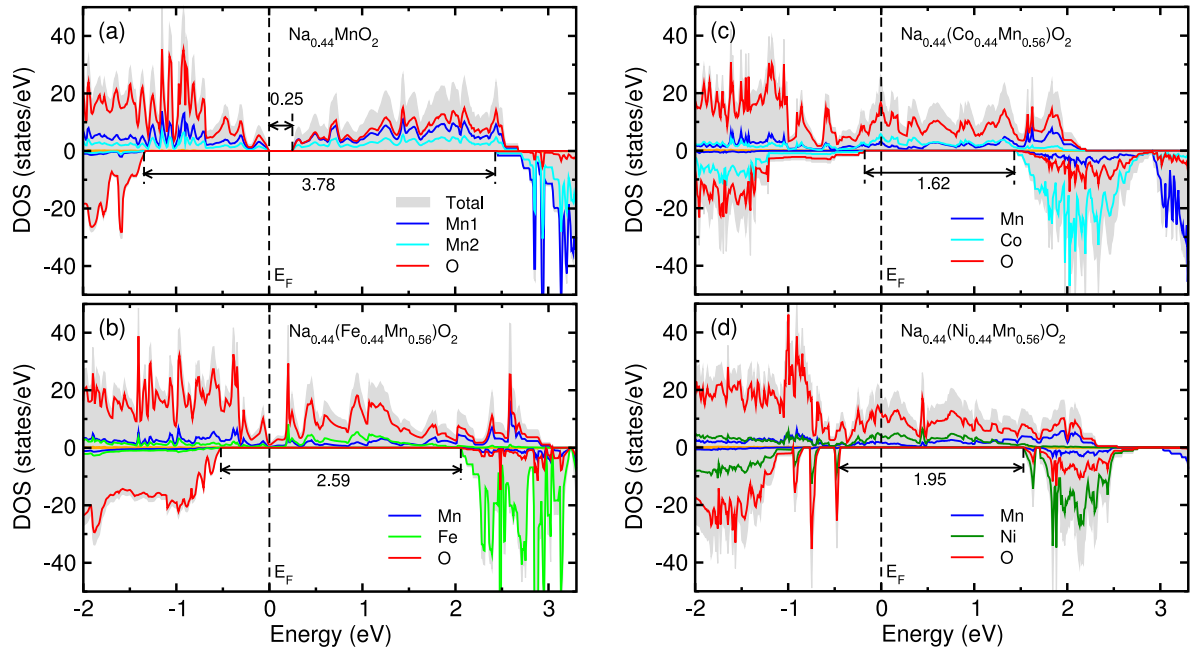

Fig. 7. Atom-resolved density of states (DOS) for $Na_{0.44}(Mn_{0.44}M_{0.56})O_2$ (M = Mn, Fe, Co, Ni), calculated with GGA+*U* method and ferromagnetic spin configuration. The Fermi level is set to zero in each case, and energy gaps are marked. The electronic states around the Fermi level are originated from 3*d* states for TM atoms and from 2*p* states for oxygen atoms. Very narrow or no band gaps are observed for spin up channel and wide band gaps for spin down channel, indicating that NMMO compounds belong to half-metallic ferromagnetic material.

4. Conclusions

In summary, we have proposed a new kind of cathode materials based on sodium manganese oxide $Na_{0.44}MnO_2$ and replacement of some Mn atoms by other TM atoms, resulting in the mixing compounds $Na_x(M_{0.44}Mn_{0.56})O_2$ (M = Mn, Fe, Co, Ni) for high voltage and high capacity cathodes of SIBs. We have applied first-principles method (GGA+*U*) within the DFT framework to investigate their electrochemical properties as varying the Na content *x* between 0.11 and 0.67. Our calculations revealed that as increasing the Na content, the cell volumes gradually increase without any anomaly despite somewhat zigzag change trend of lattice constants, and the relative volume expansion rates are under 5%, indicating their high cycling stabilities. It was found that these mixed compounds can be safely formed from the constituent

binary metal oxides due to their negative formation energies (except $Na_{0.11}MnO_2$), which increase in magnitude as increasing the number of inserting Na atoms for the four TM mixing cases. The binding strength between the host of $Na_{0.11}$MMO and inserting Na atoms was assessed by calculating the formation and binding energies, revealing the gradual decrease with increasing Na content. For these energetics, the systematic increasing tendency as increasing the atomic number of TM elements, *i.e.* going Mn→Fe→Co→Ni, was confirmed, verifying the range of Na content x. With identifying the intermediate phases during Na insertion/extraction via convex hull plot of formation enthalpies, we found that the electrode voltage ranges increase systematically as going from Mn to Ni, implying that higher energy density can be realized by intermixing, together with higher specific capacity up to 165 mAh g^{-1} than 129 mAh g^{-1} of NMO. Regarding the Na-ion diffusion, we identified the 3 different pathways for 1D channel migration within the tunnels and another one for crossing the tunnels by ΔBVS analysis, and determined the activation barriers with diffusion lengths by NEB calculations, finding very fast channel within the S-shaped tunnel and moderate one within small-sized tunnel. The activation barriers were found to slightly increase by mixing with Fe, Co and in particular Ni. From the analysis of DOS, it turned out that these compounds belong to half-metallic ferromagnetic materials with no band gaps for spin up and wide band gaps for spin down states, and moreover, the spin down band gap was found to decrease from 3.78 eV for NMO to, *e.g.*, 1.62 eV for Co mixing case, indicating the enhancement of metallicity by mixing with higher valent TM elements. We believe that this work will contribute to optimizing the cathode materials based on NMO for developing high performance SIBs.

CRediT authorship contribution statement

Chol-Jun Yu: Conceptualization, Methodology, Writing – original draft. **Yong-Chol Pak:** Data curation. **Chung-Hyok Kim:** Visualization. **Jin-Song Kim:** Investigation. **Kum-Chol Ri:** Writing – review & editing, Software. **Kwang-Hyok Ri:** Data curation. **Song-Hyok Choe:** Validation. **Stefaan Cottenier:** Supervision.

Declaration of competing interest

The authors declare that they have no known competing financial interests or personal relationships that could have appeared to influence the work reported in this paper.

Acknowledgements

This work is supported as part of the research project "Design of New Energy Materials" (No. 2021-12) by the State Commission of Science and Technology, DPR Korea. Computations have been performed on the HP Blade System C7000 (HP BL460c), which is managed by Faculty of Materials Science, Kim Il Sung University.

Appendix A. Supplementary data

Supplementary material related to this article can be found online at https://doi.org/10.1016/j.jpowsour.2021.230395.

References

[1] Y. Zhang, N. Liu, Nanostructured electrode materials for high-energy rechargeable Li, Na and Zn batteries, Chem. Mater. 29 (2017) 9589–9604.
[2] S.P. Ong, V.L. Chevrier, G. Hautier, A. Jain, C. Moore, S. Kim, X. Ma, G. Ceder, Voltage, stability and diffusion barrier differences between sodium-ion and lithium-ion intercalation materials, Energy Environ. Sci. 4 (2011) 3680–3688.
[3] Z. Zhao, Z. Yi, H. Li, R. Pathak, Z. Yang, X. Wang, Q. Qiao, Synergetic effect of spatially separated dual co-catalyst for accelerating multiple conversion reaction in advanced lithium sulfur batteries, Nano Energy 81 (2021) 105621–105624.
[4] Z. Zhao, R. Pathak, X. Wang, Z. Yang, H. Li, Q. Qiao, Sulfiphilic FeP/rGO as a highly efficient sulfur host for propelling redox kinetics toward stable lithium-sulfur battery, Electrochim. Acta 364 (2020) 137117–137148.
[5] C. Vaalma, D. Buchholz, M. Weil, S. Passerini, A cost and resource analysis of sodium-ion batteries, Nat. Rev. Mater. 3 (2018) 18013.
[6] J.-Y. Hwang, S.-T. Myung, Y.-K. Sun, Sodium-ion batteries: Present and future, Chem. Soc. Rev. 46 (2017) 3529–3614.
[7] L. Li, Y. Zheng, S.L. Zhang, J.P. Yang, Z.P. Shao, Z.P. Guo, Recent progress on sodium ion batteries: Potential high-performance anodes, Energy Environ. Sci. 11 (2018) 2310–2340.
[8] L.P. Wang, L. Yu, X. Wang, M. Srinivasan, Z.J. Xu, Recent developments in electrode materials for sodium ion batteries, J. Mater. Chem. A 3 (2015) 9353–9378.
[9] X. Xiang, K. Zhang, J. Chen, Recent advances and prospects of cathode materials for sodium-ion batteries, Adv. Mater. 27 (2015) 5343–5364.
[10] Z. Chen, T. Yuan, X. Pu, H. Yang, X. Ai, Y. Xia, Y. Cao, Symmetric sodium-ion capacitor based on $Na_{0.44}MnO_2$ nanorods for low-cost and high-performance energy storage, ACS Appl. Mater. Interfaces 10 (2018) 11689–11698.
[11] Y. Cao, L. Xiao, W. Wang, D. Choi, Z. Nie, J. Yu, L.V. Saraf, Z. Yang, J. Liu, Reversible sodium ion insertion in single crystalline manganese oxide nanowires with long cycle life, Adv. Mater. 23 (2011) 3155–3160.
[12] X. Ju, H. Huang, H. Zheng, P. Deng, S. Li, B. Qu, T. Wang, A facile method to hunt for durable high-rate capability $Na_{0.44}MnO_2$, J. Power Sources 395 (2018) 395–402.
[13] G. Ma, Y. Zhao, K. Huang, Z. Ju, C. Liu, Y. Hou, Z. Xing, Effects of the starting materials of $Na_{0.44}MnO_2$ cathode materials on their electrochemical properties for Na-ion batteries, Electrochim. Acta 222 (2016) 36–43.
[14] C.H. Wang, Y.W. Yeh, N. Wongittharom, Y.C. Wang, C.J. Tseng, S.W. Lee, W.S. Chang, J.K. Chang, Rechargeable Na/$Na_{0.44}MnO_2$ cells with ionic liquid electrolytes containing various sodium solutes, J. Power Sources 274 (2015) 1016–1023.
[15] L. Zhao, J. Ni, H. Wang, L. Gao, $Na_{0.44}MnO_2$-CNT electrodes for non-aqueous sodium batteries, RSC Adv. 3 (2013) 6650–6655.
[16] F. Sauvage, L. Laffont, J.M. Tarascon, E. Baudrin, Study of the insertion/deinsertion mechanism of sodium into $Na_{0.44}MnO_2$, Inorg. Chem. 46 (2007) 3289–3294.
[17] B. Fu, X. Zhou, Y. Wang, High-rate performance electrospun $Na_{0.44}MnO_2$ nanofibers as cathode material for sodium-ion batteries, J. Power Sources 310 (2016) 102–108.
[18] M. Xu, Y. Niu, C. Chen, J. Song, S. Bao, C.M. Li, Synthesis and application of ultra-long $Na_{0.44}MnO_2$ submicron slabs as a cathode material for Na-ion batteries, RSC Adv. 4 (2014) 38140–38143.
[19] X. Zhou, R.K. Guduru, P. Mohanty, Synthesis and characterization of $Na_{0.44}MnO_2$ from solution precursors, J. Mater. Chem. A 1 (2013) 2757–2761.
[20] R. Ruffo, R. Fathi, D.J. Kim, Y.H. Jung, C.M. Mari, D.K. Kim, Impedance analysis of $Na_{0.44}MnO_2$ positive electrode for reversible sodium batteries in organic electrolyte, Electrochim. Acta 108 (2013) 575–582.
[21] K.Y. Shen, L. Miklos, L. Wang, R.L. Axelbaum, Spray pyrolysis and electrochemical performance of $Na_{0.44}MnO_2$ for sodium-ion battery cathodes, MRS Commun. 7 (2017) 74–77.
[22] R. Qiao, K. Dai, J. Mao, T.-C. Weng, D. Sokaras, D. Nordlund, X. Song, V.S. Battaglia, Z. Hussain, G. Liu, W. Yang, Revealing and suppressing surface Mn(II) formation of $Na_{0.44}MnO_2$ electrodes for Na-ion batteries, Nano Energy 16 (2015) 186–195.
[23] K. Dai, J. Mao, X. Song, V. Battaglia, G. Liu, $Na_{0.44}MnO_2$ with very fast sodium diffusion and stable cycling synthesized via polyvinylpyrrolidone-combustion method, J. Power Sources 285 (2015) 161–168.
[24] Q. Liu, Z. Hu, M. Chen, Q. Gu, Y. Dou, Z. Sun, S. Chou, S.X. Dou, Multiangular rod-shaped $Na_{0.44}MnO_2$ as cathode materials with high rate and long life for sodium-ion batteries, ACS Appl. Mater. Interfaces 9 (2017) 3644–3652.
[25] P. Zhan, S. Wang, Y. Yuan, K. Jiao, S. Jiao, Facile synthesis of nanorod-like single crystalline $Na_{0.44}MnO_2$ for high performance sodium-ion batteries, J. Electrochem. Soc. 162 (2015) A1028–A1032.
[26] E. Hosono, T. Saito, J. Hoshino, M. Okubo, Y. Saito, D. Nishio-Hamane, T. Kudo, H. Zhou, High power Na-ion rechargeable battery with single-crystalline $Na_{0.44}MnO_2$ nanowire electrode, J. Power Sources 217 (2012) 43–46.
[27] Y. Wang, J. Liu, B. Lee, R. Qiao, Z. Yang, S. Xu, X. Yu, L. Gu, Y.-S. Hu, W. Yang, K. Kang, H. Li, X.-Q. Yang, L. Chen, X. Huang, Ti-substituted tunnel-type $Na_{0.44}MnO_2$ oxide as a negative electrode for aqueous sodium-ion batteries, Nature Commun. 6 (2015) 6401.
[28] H. Kim, D.J. Kim, D.H. Seo, M.S. Yeom, K. Kang, D.K. Kim, Y. Jung, Ab initio study of the sodium intercalation and intermediate phases in $Na_{0.44}MnO_2$ for sodium-ion battery, Chem. Mater. 24 (2012) 1205–1211.
[29] V. Dall'Asta, D. Buchholz, L.G. Chagas, X. Dou, C. Ferrara, E. Quartarone, C. Tealdi, S. Passerini, Aqueous processing of $Na_{0.44}MnO_2$ cathode material for the development of greener Na-ion batteries, ACS Appl. Mater. Interfaces 9 (2017) 34891–34899.
[30] Z. Li, D. Young, K. Xiang, W.C. Carter, Y.M. Chiang, Towards high power high energy aqueous sodium-ion batteries: The $NaTi_2(PO_4)_3$/$Na_{0.44}MnO_2$ system, Adv. Energy Mater. 3 (2013) 290–294.

[31] D.J. Kim, R. Ponraj, A.G. Kannan, H.W. Lee, R. Fathi, R. Ruffo, C.M. Mari, D.K. Kim, Diffusion behavior of sodium ions in $Na_{0.44}MnO_2$ in aqueous and non-aqueous electrolytes, J. Power Sources 244 (2013) 758–763.

[32] D. Nayak, P.K. Jha, S. Ghosh, V. Adyam, Aluminium substituted β-type $NaMn_1 - xAl_xO_2$: A stable and enhanced electrochemical kinetic sodium-ion battery cathode, J. Power Source 438 (2019) 227025–227032.

[33] D. Nayak, T. Sarkar, N. Vijay, P. Chaudhary, M.D. Bharadwaj, S. Ghosh, V. Adyam, Electrochemical properties and first-principles analysis of $Na_x[M_yMn_1 - y]O_2$ (M = Fe, Ni) cathode, J. Solid State Electrochem. 22 (2018) 1079–1089.

[34] I. Hasa, D. Buchholz, S. Passerini, J. Hassoun, A comparative study of layered transition metal oxide cathodes for application in sodium-ion battery, ACS Appl. Mater. Interfaces 7 (2015) 5206–5212.

[35] D.D. Yuan, Y.X. Wang, Y.L. Cao, X.P. Ai, H.X. Yang, Improved electrochemical performance of Fe-substituted $NaNi_{0.5}Mn_{0.5}O_2$ cathode materials for sodium-ion batteries, ACS Appl. Mater. Interfaces 7 (2015) 8585–8591.

[36] W.K. Pang, S. Kalluri, V.K. Peterson, N. Sharma, J. Kimpton, B. Johannessen, H.K. Liu, S.X. Dou, Z. Guo, Interplay between electrochemistry and phase evolution of the P2-type $Na_x(Fe_1/2Mn_{1/2})O_2$ cathode for use in sodium-ion batteries, Chem. Mater. 27 (2015) 3150–3158.

[37] J. Zhao, J. Xu, D.H. Lee, N. Dimov, Y.S. Meng, S. Okada, Electrochemical and thermal properties of P2-type $Na_2/3Fe_{1/3}Mn_{2/3}O_2$ for Na-ion batteries, J. Power Sources 264 (2014) 235–239.

[38] C.-J. Yu, S.-G. Hwang, Y.-C. Pak, S.-H. Choe, J.-S. Kim, K.-C. Ri, Influence of Ti/V cation-exchange in $Na_2Ti_3O_7$ on Na-ion negative electrode performance: An insight from first-principles study, J. Phys. Chem. C 124 (2020) 17897–17906.

[39] N. Yabuuchi, R. Hara, K. Kubota, J. Paulsen, S. Kumakura, S. Komaba, A new electrode material for rechargeable sodium batteries: P2-type $Na_2/3Mg_{0.28}Mn_{0.72}O_2$ with anomalously high reversible capacity, J. Mater. Chem. A 2 (2014) 16851–16855.

[40] Y. Wen, B. Wang, G. Zeng, K. Nogita, D. Ye, L. Wang, Electrochemical and structural study of layered P2-type $Na_2/3Ni_{1/3}Mn_{2/3}O_2$ as cathode material for sodium-ion battery, Chem. Asian J. 10 (2015) 661–666.

[41] S. Komaba, N. Yabuuchi, T. Nakayama, A. Ogata, T. Ishikawa, I. Nakai, Study on the reversible electrode reaction of $Na_{1-x}Ni_{0.5}Mn_{0.5}O_2$ for a rechargeable sodium-ion battery, Inorg. Chem. 51 (2012) 6211–6220.

[42] N. Yabuuchi, M. Kajiyama, J. Iwatate, H. Nishikawa, S. Hitomi, R. Okuyama, R. Usui, Y. Yamada, S. Komaba, P2-type $Na_x[Fe_1/2Mn_{1/2}]O_2$ made from earth-abundant elements for rechargeable Na batteries, Nature Mater. 11 (2012) 512–517.

[43] S. Xu, Y. Wang, L. Ben, Y. Lyu, N. Song, Z. Yang, Y. Li, L. Mu, H.-T. Yang, L. Gu, Y.-S. Hu, H. Li, Z.-H. Cheng, L. Chen, X. Huang, Fe-based tunnel-type $Na_{0.61}Mn_{0.27}Fe_{0.34}Ti_{0.39}O_2$ designed by a new strategy as a cathode material for sodium-ion batteries, Adv. Energy Mater. 5 (2015) 1501156.

[44] I. Hasa, D. Buchholz, S. Passerini, B. Scrosati, J. Hassoun, High performance $Na_{0.5}[Ni_{0.23}Fe_{0.13}Mn_{0.63}]O_2$ cathode for sodium-ion batteries, Adv. Energy Mater. 4 (2014) 1400083.

[45] M. Huon Han, E. Gonzalo, N. Sharma, J. Miguel Lopez del Amo, M. Armand, M. Avdeev, J.J. Saiz Garitaonandia, T. Rojo, High-performance P2-phase $Na_2/3Mn_{0.8}Fe_{0.1}Ti_{0.1}O_2$ cathode material for ambient-temperature sodium-ion batteries, Chem. Mater. 28 (2016) 106–116.

[46] P. Vassilaras, A.J. Toumar, G. Ceder, Electrochemical properties of $NaNi_1/3Co_{1/3}Fe_{1/3}O_2$ as a cathode material for na-ion batteries, Electrochem. Commun. 38 (2014) 79–81.

[47] D. Kim, E. Lee, M. Slater, W. Lu, S. Rood, C.S. Johnson, Layered $Na[Ni_1/3Fe_{1/3}Mn_{1/3}]O_2$ cathodes for Na-ion battery application, Electrochem. Commun. 18 (2012) 66–69.

[48] X. Li, D. Wu, Y.-N. Zhou, L. Liu, X.-Q. Yang, G. Ceder, O3-type $Na(Mn_{0.25}Fe_{0.25}Co_{0.25}Ni_{0.25})O_2$: A quaternary layered cathode compound for rechargeable Na ion batteries, Electrochem. Commun. 49 (2014) 51–54.

[49] R.C. Longo, F. Kong, C. Liang, D.-H. Yeon, J. Yoon, J.-H. Park, S.-G. Doo, K. Cho, Transition metal ordering optimization for high-reversible capacity positive electrode materials in the Li-Ni-Co-Mn pseudoquaternary system, J. Phys. Chem. C 120 (2016) 8540–8549.

[50] Q. Zhang, W. Wang, Y. Wang, P. Feng, K. Wang, S. Cheng, K. Jiang, Controllable construction of 3D-skeleton-carbon coated $Na_3V_2(PO_4)_3$ for high-performance sodium ion battery cathode, Nano Energy 20 (2016) 11–19.

[51] S.T. Dacek, W.D. Richards, D.A. Kitchaev, G. Ceder, Structure and dynamics of fluorophosphate Na-ion battery cathodes, Chem. Mater. 28 (2016) 5450–5460.

[52] P. Moreau, D. Guyomard, J. Gaubicher, F. Boucher, Structure and stability of sodium intercalated phases in olivine $FePO_4$, Chem. Mater. 22 (2010) 4126–4128.

[53] G. Hautier, A. Jain, H. Chen, C. Moore, S.P. Ong, G. Ceder, Novel mixed polyanions lithium-ion battery cathode materials predicted by high-throughput Ab initio computations, J. Mater. Chem. 21 (2011) 17147–17153.

[54] G. Yan, S. Mariyappan, G. Rousse, Q. Jacquet, M. Deschamps, R. David, B. Mirvaux, J.W. Freeland, J.-M. Tarascon, Higher energy and safer sodium ion batteries via an electrochemically made disordered Na3V2(PO4)2F3 material, Nature Commun. 10 (2019) 585.

[55] C.-J. Yu, S.-H. Choe, G.-C. Ri, S.-C. Kim, H.-S. Ryo, Y.-J. Kim, Ionic diffusion and electronic transport in eldfellite $Na_xFe(SO_4)_2$, Phys. Rev. Appl. 8 (2017) 024029.

[56] G.-C. Ri, S.-H. Choe, C.-J. Yu, First-principles study of mixed eldfellite compounds $Na_x(Fe_1/2M_{1/2})(SO_4)_2$ (x = 0-2, M = Mn, Co, Ni): a new family of high electrode potential cathodes for the sodium-ion battery, J. Power Sources 378 (2018) 375–382.

[57] P. Barpanda, G. Oyama, S. Nishimura, S. Chung, A. Yamada, A 3.8-V earth-abundant sodium battery electrode, Nature Commun. 5 (2014) 4358.

[58] A. Banerjee, R.B. Araujo, R. Ahuja, Unveiling the thermodynamic and kinetic properties of $Na_xFe(SO_4)_2$ (x = 0–2): toward a high capacity and low-cost cathode material, J. Mater. Chem. A 4 (2016) 17960–17969.

[59] L. Li, L. Zhu, L.-H. Xu, T.-M. Cheng, W. Wang, X. Li, Q.-T. Sui, Site-exchange of li and m ions in silicate cathode materials Li2MSiO4 (M = Mn, Fe, Co and Ni): DFT calculations, J. Mater. Chem. A 2 (2014) 4251–4255.

[60] Crystallographic Database, http://crystallography.net/cod/2107994.html.

[61] W. Mumme, The structure of $Na_4Mn_4Ti_5O_{18}$, Acta Crystallogr. B 24 (1968) 1114–1120.

[62] P. Giannozzi, S. Baroni, N. Bonini, M. Calandra, R. Car, C. Cavazzoni, D. Ceresoli, L.C. Guido, M. Cococcioni, I. Dabo, A.D. Corso, S. Fabris, G. Fratesi, S. de Gironcoli, R. Gebauer, U. Gerstmann, C. Gougoussis, A. Kokalj, M. Lazzeri, L. Martin-Samos, N. Marzari, F. Mauri, R. Mazzarello, S. Paolini, A. Pasquarello, L. Paulatto, C. Sbraccia, S. Scandolo, G. Sclauzero, A.P. Seitsonen, A. Smogunov, P. Umari, R.M. Wentzcovitch, QUANTUM ESPRESSO: a modular and open-source software project for quantum simulations of materials, J. Phys.: Condens. Matter 21 (2009) 395502.

[63] J.P. Perdew, K. Burke, M. Ernzerhof, Generalized gradient approximation made simple, Phys. Rev. Lett. 77 (1996) 3865.

[64] M. Cococcioni, S. de Gironcoli, Linear response approach to the calculation of the effective interaction parameters in the LDA + U method, Phys. Rev. B 71 (2005) 035105.

[65] F. Zhou, M. Cococcioni, C.A. Marianetti, D. Morgan, G. Ceder, First-principles prediction of redox potentials in transition-metal compounds with LDA+U, Phys. Rev. B 70 (2004) 235121.

[66] S. Adam, From bond valence maps to energy landscapes for mobile ions in ion-conducting solids, Solid State Ion. 177 (2006) 1625–1630.

[67] L.L. Wong, H. Chen, S. Adams, Design of fast ion conducting cathode materials for grid-scale sodium-ion batteries, Phys. Chem. Chem. Phys. 19 (2017) 7506–7523.

[68] G. Henkelman, B.P. Uberuaga, H. Jónsson, A climbing image nudged elastic band method for finding saddle points and minimum energy paths, J. Chem. Phys. 113 (2000) 9901–9904.

[69] K. Momma, F. Izumi, VESTA 3 for three-dimensional visualization of crystal, volumetric and morphology data, J. Appl. Crystallogr. 44 (2011) 1272–1276.

[70] D.R. Lide (Ed.), CRC Handbook of Chemistry and Physics, Internet Version 2005, CRC Press, http://www.hbcpnetbase.com, Boca Raton, FL, 2005.

[71] S. Muhammady, Y. Kurniawan, A. Rusydi, Y. Darma, Electronic and magnetic properties of new half-metallic ferromagnetic rutile $Ti,1 - x - yV,xNi,yO2$ ($x = y$ = 6.25%): A first-principles study, J. Phys. Chem. Solids 125 (2018) 16–22.

[72] R. Luo, F. Wu, M. Xie, Y. Ying, J. Zhou, Y. Huang, Y. Ye, L. Li, R. Chen, Habit plane-driven P2-type manganese-based layered oxide as long cycling cathode for Na-ion batteries, J. Power Sources 383 (2018) 80–86.

[73] R. Arras, L. Calmels, B. Warot-Fonrose, Half-metallicity, magnetic moments, and gap states in oxygen-deficient magnetite for spintronic applications, Appl. Phys. Lett. 100 (2012) 032403.